

Short Note

(2R,4aS,6aS,12bR,14aS,14bR)-N-(2-(2-(2-(2-Azidoethoxy)ethoxy)ethyl)-10-hydroxy-2,4a,6a,9,12b,14a-hexamethyl-11-oxo-1,2,3,4,4a,5,6,6a,11,12b,13,14,14a,14b-tetradecahydropicene-2-carboxamide

Guo Yuzhu¹, Margrate Anyanwu², Xiao Yang¹, Ren Zimo¹, Alessandra Gianoncelli², Giovanni Ribaldo^{2,*}
and Paolo Coghi^{1,3,*}

¹ School of Pharmacy, Macau University of Science and Technology, Macau 999078, China; 2009853tpa11001@student.must.edu.mo (G.Y.); 2009853dpa11004@student.must.edu.mo (X.Y.), 2230028575@student.must.edu.mo (R.Z.)

² Department of Molecular and Translational Medicine, University of Brescia, 25123 Brescia, Italy; margrate.anyanwu@unibs.it (M.A.); alessandra.gianoncelli@unibs.it (A.G.)

³ State Key Laboratory of Quality Research in Chinese Medicine, Science and Technology Building, Macau University of Science and Technology, Avenida Wai Long, Taipa, Macau 999078, China

* Correspondence: giovanni.ribaldo@unibs.it (G.R.); coghips@must.edu.mo (P.C.); Tel.: +853-88972853 (P.C.)

Abstract: In this report, we discuss the synthesis of a compound obtained from the derivatization of the natural compound celastrol. This derivative is connected to PEG azide moiety through an amide linkage. The linkage was achieved through the activation of the carboxylic acid using HOBt/EDC. The compound was fully characterized by proton (¹H), carbon-13 (¹³C), heteronuclear single quantum coherence (HSQC), correlation spectroscopy (¹H-¹H-COSY), and distortionless enhancement by polarization transfer (DEPT) NMR. Ultraviolet (UV), Fourier-transform infrared (FTIR), and high-resolution mass spectrometry (HRMS) were also adopted. Computational investigations were conducted to forecast the binding mode between the synthesized compound and sarco-endoplasmic reticulum (SR) Ca²⁺ transport ATPase (SERCA), a known target for the development of novel therapeutics for rheumatoid arthritis. Additionally, the drug-likeness of the synthesized compound was assessed by predicting its pharmacokinetic properties.

Keywords: celastrol; PEG; SERCA; rheumatoid arthritis; molecular docking; drug discovery



Citation: Yuzhu, G.; Anyanwu, M.; Yang, X.; Zimo, R.; Gianoncelli, A.; Ribaldo, G.; Coghi, P.

(2R,4aS,6aS,12bR,14aS,14bR)-N-(2-(2-(2-(2-Azidoethoxy)ethoxy)ethyl)-10-hydroxy-2,4a,6a,9,12b,14a-hexamethyl-11-oxo-1,2,3,4,4a,5,6,6a,11,12b,13,14,14a,14b-tetradecahydropicene-2-carboxamide. *Molbank* **2024**, *2024*, M1800. <https://doi.org/10.3390/M1800>

Academic Editor: Nicholas Leadbeater

Received: 5 March 2024

Revised: 28 March 2024

Accepted: 30 March 2024

Published: 1 April 2024



Copyright: © 2024 by the authors. Licensee MDPI, Basel, Switzerland. This article is an open access article distributed under the terms and conditions of the Creative Commons Attribution (CC BY) license (<https://creativecommons.org/licenses/by/4.0/>).

1. Introduction

Recently, celastrol (**1**) has gained prominence as a drug candidate because of its potential therapeutic properties. Sourced from the roots of *Tripterygium wilfordii*, a traditional Chinese medicinal plant steeped in centuries-old practices of traditional Chinese medicine, **1** has become a focal point for scientific exploration. Although **1** has been part of traditional Chinese medical culture for the treatment of various disorders for several generations, this molecule has only gained importance in the last ten years due to its beneficial pharmacological effects, as revealed by investigations on its molecular mechanisms undertaken during this period.

Notably, **1** exhibits a multitude of beneficial properties, including anti-inflammatory [1], antioxidant [2], cardioprotective [3], and anti-rheumatic activities [4]. Additionally, celastrol has demonstrated anticancer activity [5], as well as efficacy in combating neuronal degeneration [6] and addressing obesity [7]. Certainly, one of the most captivating features of compound **1** is its capacity to regulate cellular signaling pathways pivotal in disease advancement. Studies have shown that celastrol can inhibit the activation of nuclear factor-kappa B (NF- κ B) [8], Hsp90-Cdc37 [9] and sarco-endoplasmic reticulum (SR) Ca²⁺ transport ATPase (SERCA) [10].

Rheumatoid arthritis (RA) is a systemic, chronic, autoimmune inflammatory disease that primarily affects the joints. This condition has a worldwide prevalence that ranges from 0.25% to 1% [11]. Given the debilitating nature of this condition, many efforts have been made to find a definitive solution, capable of alleviating the symptoms. The pathogenesis of RA is complex and not fully understood, since a variety of cell populations (e.g., macrophages, lymphocytes, and fibroblasts) and molecules are involved in these mechanisms [12]. Among these, Ca^{2+} has a pivotal function, since it plays a role in autoimmunity and the consequent progress of the disease [13]. One of the effectors dependent on the presence of Ca^{2+} is the sarcoplasmic/endoplasmic reticulum (SR/ER) Ca^{2+} -ATPase (SERCA). The importance of this protein has also manifested itself at the level of other pathologies, such as in tumors. In this extent, research has shown that SERCA inhibitors (e.g., thapsigargin) prompt the accumulation of cytosolic and mitochondrial Ca^{2+} , along with ATP depletion, potentially triggering various signaling pathways that culminate in the demise of cancer cells [14]. Additionally, SERCA is a noteworthy anti-arthritic target [10,15]. Several studies report that its pharmacological inhibition led to beneficial effects in the field of RA [16]. To this end, celastrol was investigated for SERCA inhibition, since it was reported to reduce bone damage and suppress autoimmune arthritis [10].

Despite the fact that celastrol shows a promising potential, further research is needed to fully understand its mechanisms of action and side effects, since its therapeutic benefits are recognized, but at the same time, certain drawbacks including elevated toxicity, limited water solubility, and stability issues, limit its broader clinical use.

To overcome these limitations, medicinal chemists have shown interest in organic synthetic and semi-synthetic approaches to produce novel celastrol active derivatives (Figure 1, panel ii). Simple modifications, such as esterification or amidation of the C29-carboxylic acid (Figure 1, panel i), were employed to improve solubility, mitigate toxicity, and discover new activities of celastrol analogues [17–19]. Further, to improve the efficacy of these new analogues, targeted nanodelivery systems are under development [20]. These innovative approaches aim to regulate drug release and bioavailability, as well as reduce systemic toxicity. Several strategies are implied in this context, including the use of nanoparticles (NPs), liposomes, and micelles. The process of chemically linking an insoluble drug with a hydrophilic polymer can induce self-assembly into NPs, thereby enhancing the apparent solubility and optimizing the drug's pharmacokinetics. The PEG azide nanodelivery system demonstrates enhanced efficiency in targeted drug delivery, highlighting its potential for therapeutic applications [21].

In this context, this study elucidates the synthesis and computational investigations of a celastrol derivative, wherein the scaffold has been intricately linked to a specific moiety, PEG azide (3) (Figure 1). A future application could be the use of this derivative to perform profiling studies. This could be performed by coupling this analogues to biotin linkers through the Staudinger–Bertozzi reaction [22,23] or by using click chemistry [24], conjugating various molecular weights of short-chain PEG to a small molecule drug.

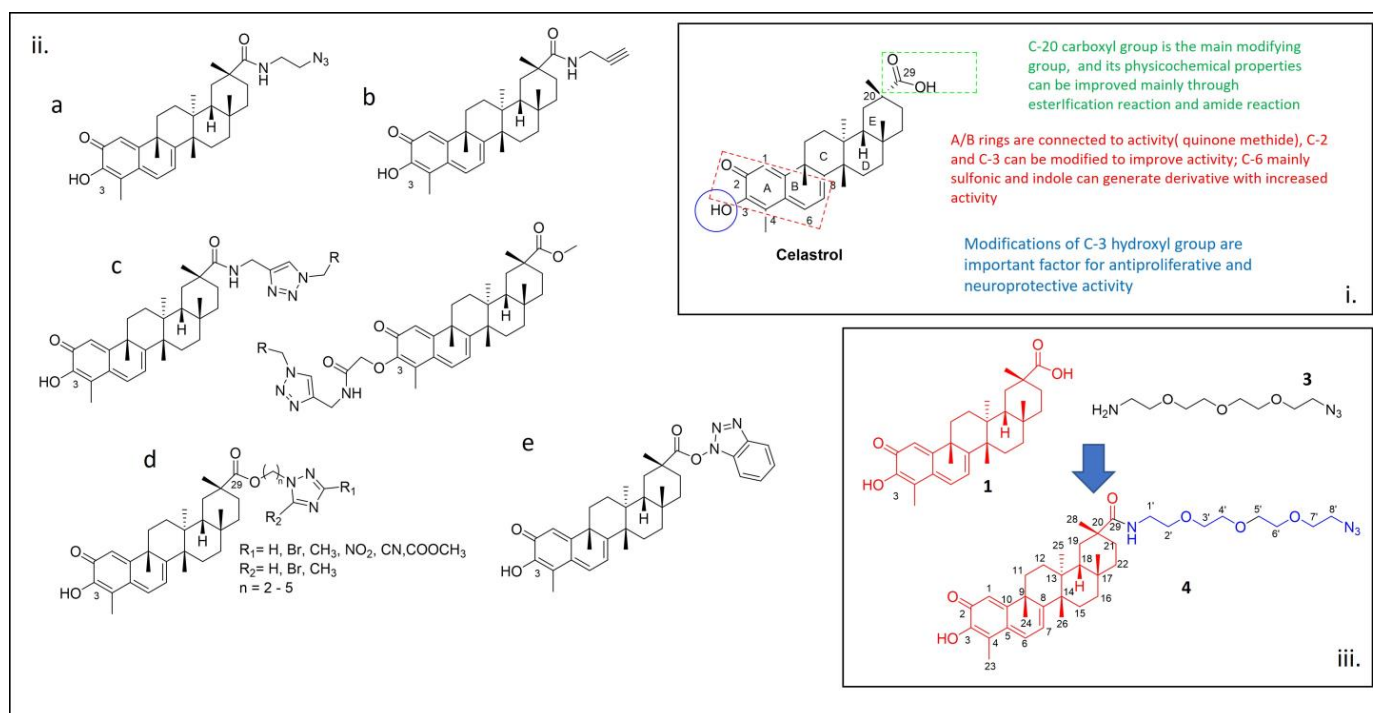
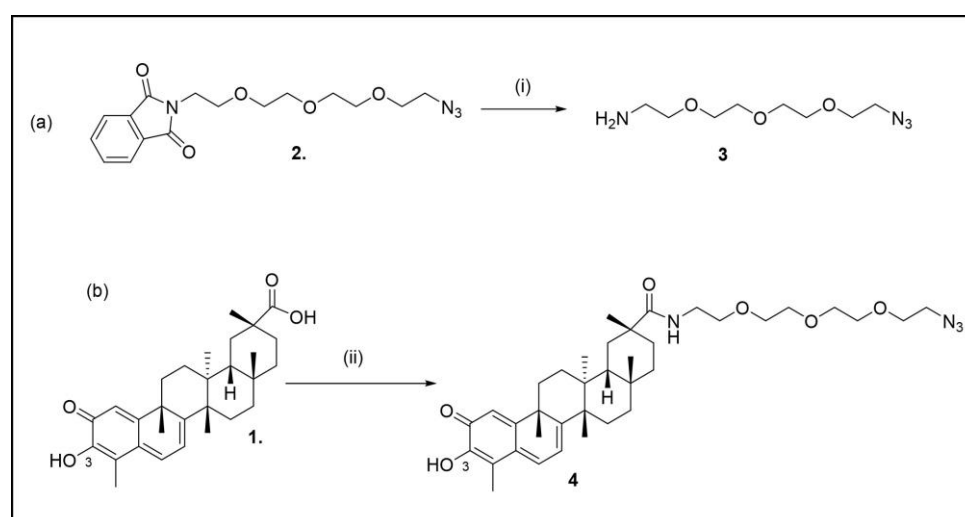


Figure 1. (i) Functional groups of celastrol (**1**) that are important for its biological activity. (ii) Example of celastrol derivatives reported in the literature: (a) [17], (b) [25] and 1,2,3 and 1,2,4-triazol celastrol derivatives, (c) [26], (d) [27], and (e) [28]. (iii) Chemical structures of 11-Azido-3,6,9-trioxaundecan-1-amine (**3**) and compound **4** are reported in the inset of the figure.

2. Results and Discussion

The synthetic route for (2R,4aS,6aS,12bR,14aS,14bR)-N-(2-(2-(2-(2-azidoethoxy)ethoxy)ethoxy)ethyl)-10-hydroxy-2,4a,6a,9,12b,14a-hexamethyl-11-oxo-1,2,3,4,4a,5,6,6a,11,12b,13,14,14a,14b-tetradecahydronicene-2-carboxamide started from the preparation of the precursor (**3**, Scheme 1a).



Scheme 1. (a) Synthesis of 11-Azido-3,6,9-trioxaundecan-1-amine **3** (i) ethanol, hydrazine monohydrate, 4 h, 85 °C. (b) Synthesis of (2R,4aS,6aS,12bR,14aS,14bR)-N-(2-(2-(2-(2-azidoethoxy)ethoxy)ethoxy)ethyl)-10-hydroxy-2,4a,6a,9,12b,14a-hexamethyl-11-oxo-1,2,3,4,4a,5,6,6a,11,12b,13,14,14a,14b-tetradecahydronicene-2-carboxamide (ii) **3**, EDC hydrochloride (3 equiv.), HOBT (3 equiv.), CH₂Cl₂.

Isoindoline-1,3-dione, or phthalimide, constitutes an important group of chemical compounds. It serves as a $^-NH_2$ -synthon, allowing the preparation of primary amines and is used to prepare amine PEG. In particular, following the protocol reported in the literature [29], 11-azido-3,6,9-trioxaundecan-1-amine **3** was prepared by the reaction of 2-(2-(2-(2-(2-azidoethoxy)ethoxy)ethoxy)ethyl)isoindoline-1,3-dione **2** in ethanol with hydrazine monohydrate by Gabriel synthesis. The structure of **3** was determined by 1H -, ^{13}C -NMR, and DEPT-135 spectra (Supplementary Materials, Figures S1–S3).

11-Azido-3,6,9-trioxaundecan-1-amine (**3**) was used as a starting compound by a coupling reaction using HOBt/EDC/TEA as the activation conditions using a modified protocol reported by Pang et al. [30]. EDC reagent and its urea byproduct are water soluble, so the byproducts are removed by aqueous extraction.

A solution of celastrol in CH_2Cl_2 was prepared, to which HOBt and EDC hydrochloride were added, together with three equivalents of intermediate **3** (Scheme 1, step b), and compound **4** was isolated in a high yield. Subsequently, the chemical structure of compound **4** was confirmed by NMR, IR, UV, and mass spectrometry analysis. Concerning the NMR analysis, the 1H -NMR spectrum showed peaks associated with the methylene groups 2'-6' in the region δH 3.29–3.68 ppm (Figure S4) and a peak at ppm δH 3.39 associated with azide CH_2 , thus supporting the formation of the expected product. Regarding the ^{13}C -NMR signals, the disappearance of peculiar peaks of carboxylic acid at 182 ppm of compound **1**, and the appearance of the peak at 178.3 ppm of the amide were probably the most relevant features to verify the reaction with the PEG azide (Figure S5). Of note, six signals in the region δC 70.7–69.5 123 ppm were attributed to the carbons 2'-6'.

Heteronuclear single quantum coherence spectroscopy (HSQC), correlation spectroscopy (1H - 1H -COSY), and distortionless enhancement by polarization transfer (DEPT-135, DEPT-90, and DEPT-45) were also used to assign ^{13}C signals of compound **4**, as shown in Table S1 (see Supplementary Materials for 2D spectra, Figures S6–S10). The ^{13}C -NMR spectrum of **4** exhibited 37 carbon signals were classified by DEPT experiments as six methyl groups, fifteen methylene, four methines, and twelve quaternary carbons.

The IR spectrum of compound **4** showed characteristic N–H stretching at 3332 cm^{-1} , C–H stretching at 2931 and 2870 cm^{-1} , and secondary amide stretching at 1643 cm^{-1} compared to **1** (Supplementary Materials, Figures S11 and S12). Other vibrational peaks at 1442 cm^{-1} were attributed to the O–H bending in the amide.

The stronger band found at 1288 and 1103 cm^{-1} could be assigned to the characteristic C–O stretching vibrations of the aliphatic ether group of polyethylene glycol.

Moreover, the disappearance of C=O stretching of carboxylic acid confirms the reaction at position 29 (Figure S12), while the appearance of the N=N=N stretching peak of **4** at 2106 cm^{-1} supports the presence of the azide (Figure S12).

The UV spectrum of **4** was also recorded for further characterization, showing an absorption peak at 228 nm and another lower absorption peak at 420 nm ($n \rightarrow \pi$ transition) (Supplementary Materials, Figure S13).

An HRMS value of **4** was also obtained for further characterization, validating the proposed structure determined by NMR spectra (Supplementary Materials, Figure S14).

In order to inspect whether compound **4** could be a good candidate as a SERCA inhibitor, we performed computational studies to assess its binding mode with SERCA (Figure 2).

A site-specific molecular docking technique was adopted to preliminarily investigate the interaction motif of compound **4** with SERCA. For this reason, the X-ray crystallographic structure of SERCA in complex with thapsigargin was considered (PDB ID: 1IWO) [31]. The robustness of the docking protocol used was evaluated by re-docking thapsigargin to the SERCA binding site and by comparing the docked pose (-8.6 kcal/mol) with the co-crystallized ligand. Further, a root-mean-square deviation (RMSD) value of 1.1056 \AA was obtained, hence supporting the accuracy of the protocol (Figure 2A). Then, the same protocol was adopted to evaluate the binding mode of compound **4** and celastrol into the same binding site of thapsigargin. A calculated binding energy value of -7.2 kcal/mol

was computed for compound **4** (Figure 2B), while celastrol reported a docking score of -9.6 kcal/mol (Supplementary Materials, Figure S15A,B). The studied molecule, namely compound **4**, interacts with the binding pocket targeted by thapsigargin through a partially similar binding motif. It must be noted anyway that the two compounds are chemically different and are based on different scaffolds. Nevertheless, the analysis of the docking pose demonstrates a co-localization of the hydrophobic parts of the molecules. In Figure 2B, the residues within interaction distance (<5 Å) have been labelled. As can be noted from the model, the binding pocket is indeed rich in hydrophobic residues (e.g., Ile, Leu, Val, Phe), which are targeted by both compounds.

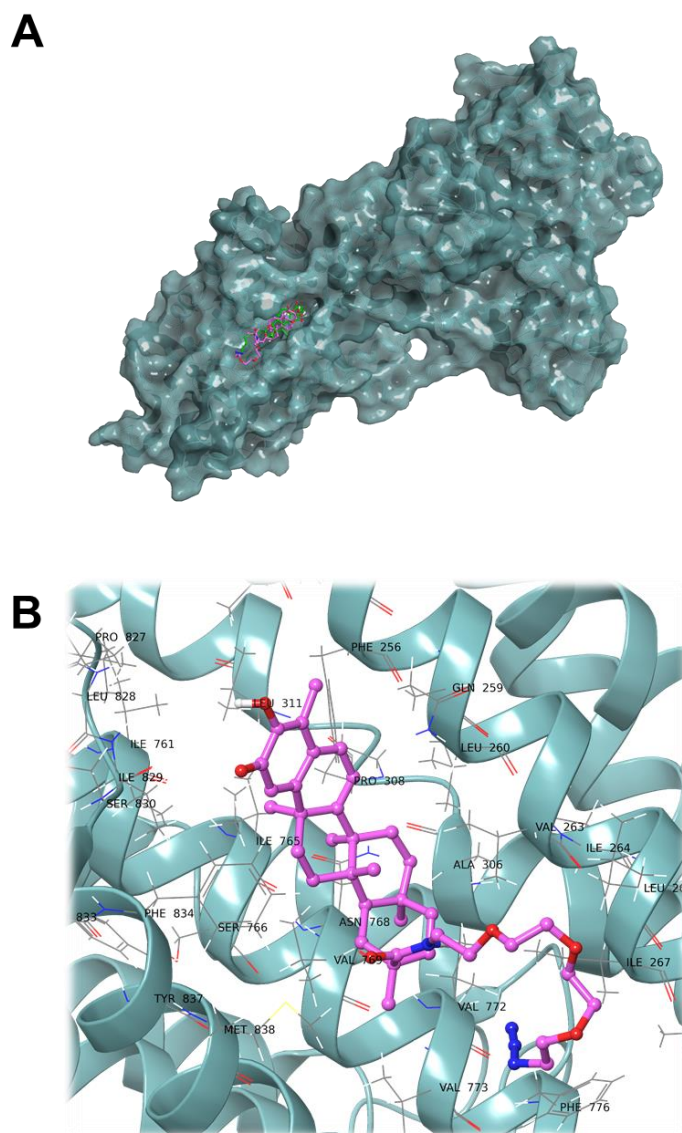


Figure 2. Predicted interaction motif for compound **4** (pink) and co-crystallized pose of thapsigargin (green) within SERCA binding site (PDB ID: 1IWO) (A). Detailed view of best-docked pose of **4** (magenta) in the binding site of SERCA. Residues located in a zone of 5 Å radius from the center of the ligand have been labeled (B).

Considering potential pharmacological uses, compound **4** underwent assessment of its physicochemical properties and oral bioavailability via ligand-based predictive modeling [32]. The analysis of these computations (Supplementary Materials, Table S2) revealed that compound **4** violates one of the parameters of the Lipinski's rule, indicating the necessity for further refinement to meet comprehensive drug-like standards. Thus, even

if the compound showed promising binding mode towards SERCA and a good binding affinity value, it may be characterized by poor bioavailability. As a consequence, parameters such as molecular weight and TPSA should be improved before further studies.

3. Materials and Methods

3.1. Chemistry

Silica gel (FCP 230–400 mesh) was used for column chromatography. Thin-layer chromatography was carried out on Merck precoated silica gel 60 F₂₅₄ plates and visualized with phosphomolybdic acid, iodine, or a UV–visible lamp.

All chemicals were purchased from Bide Pharmatech., Ltd. (Shanghai, China) and J & K scientific (Hong Kong, China). ¹H-NMR and ¹³C-NMR spectra were collected in CDCl₃ and DMSO at 25 °C on a Bruker Ascend[®]-600 NMR spectrometer (600 MHz for ¹H and 150 MHz for ¹³C). All chemical shifts were reported in the standard δ notation of parts per million using the peak of residual proton signals of CDCl₃ as an internal reference (CDCl₃, δ_C 77.2 ppm, δ_H 7.26 ppm). High resolution mass spectra (HRMS) were measured using electrospray ionization (ESI). The measurements were performed in a positive ion mode (interface capillary voltage 4500 V); the mass-to-charge ratio was set from m/z 50 to 3000 Da; external/internal calibration was conducted using electrospray calibration solution. HRMS analyses were performed by an Agilent 6230 ESI time-of-flight (TOF) mass spectrometer with Agilent C18 column (4.6 mm \times 150 mm, 3.5 μ m). The mobile phase was isocratic (water + 0.01% TFA; CH₃CN) at a flow rate of 0.35 mL/min. The peaks were determined at 254 nm using a UV detector.

UV analysis was performed on a Shimadzu UV–2600 with a 1 cm quartz cell and a slit width of 2.0 nm. The analysis was carried out using wavelengths in the range of 200–700 nm.

The FT-IR analysis was performed using a Shimadzu IRAffinity-1S (Osaka, Japan) with a frequency range of 4000–500 cm⁻¹ equipped with a SPECAC ATR accessory.

3.1.1. Synthesis of 11-Azido-3,6,9-trioxaundecan-1-amine (3)

To a solution of 2-(2-(2-(2-(2-azidoethoxy)ethoxy)ethoxy)ethyl)isoindoline-1,3-dione (0.479 g, 1.376 mmol, 1.0 eq) in ethanol (25 mL) hydrazine monohydrate (0.3480 g, 6.96 mmol, 5.0 eq) was added, and the reaction mixture was allowed to stir for 4 h at 85 °C. After cooling down to RT, the precipitate was filtered off, and the filtrate was evaporated under reduced pressure. The residue was dissolved in a small amount of ethanol (ca. 20 mL), and the solution was cooled down to 0 °C. The resulting precipitate was filtered off and the filtrate was evaporated under reduced pressure. The residue was loaded onto silica and purified by silica gel column chromatography (ethyl acetate:cyclohexane, 1:1 \rightarrow 2:1) to obtain 2-{2-[2-(2-azidoethoxy)ethoxy]ethoxy}ethan-1-amine (quantitative) as a light yellow oil. The yield was 80% δ_H (600MHz, CDCl₃) 3.70–3.63 (10H, m, H3–H7), 3.61 (2H, t, H2), 3.42 (2H, m, H8), 2.98 (2H, t, H1); δ_C (150 MHz, CDCl₃): δ = 71.6 (C2), 70.9, 70.9, 70.8, 70.5, 70.3 (C3–C7), 51 (C8), 41.4 (C1); ESI-MS m/z 219.44 [M + H]⁺ (calcd. for C₈H₁₉N₄O₃⁺, m/z 219.42).

The spectral characteristics are consistent with those of 3 in the literature [29].

3.1.2. Synthesis of (2R,4aS,6aS,12bR,14aS,14bR)10-hydroxy-N-(4-((6-methoxyquinolin-8-yl)amino)pentyl)-2,4a,6a,9,12b,14a-hexamethyl-11-oxo-1,2,3,4,4a,5,6,6a,11,12b,13,14,14a,14b-tetradecahydronicene-2-carboxamide (4)

To a CH₂Cl₂ (6 mL) solution of celastrol (45 mg, 0.10 mmol), HOBT (41 mg, 0.30 mmol) and EDC-HCl (57 mg, 0.30 mmol) were added under ice/salt-bath (5 °C) conditions. Then, Et₃N (70 μ L) was added after 20 min, and the solution was stirred at 5 °C for 1 h. Then, 3 was added, and the mixture was stirred at room temperature for 12–18 h. The mixture was washed thrice with water, and the organic phase was collected, dried over anhydrous Na₂SO₄, filtered, and concentrated in vacuo to give the crude product. The purification was implemented by chromatography on a silica gel column (eluent: from CH₂Cl₂ to 5% MeOH). The yield was 80%, δ_H (600 MHz, CDCl₃) 0.64 (3H, s, CH₃), 0.99 (1H, d, H-22),

1.12 (3H, s, CH₃), 1.15 (3H, s, CH₃), 1.26 (3H, s, CH₃), 1.44 (3H, s, CH₃), 1.49–1.70 (7H, m), 1.82–1.92 (3H, m), 1.94–2.15 (4H, m), 2.21 (3H, s, CH₃), 2.44 (1H, t, H-19), 3.29–3.34 (2H, m), 3.39 (2H, t, CH₂), 3.44–3.50 (2H, m, CH₂), 3.57–3.59 (2H, m, CH₂), 3.63–3.68 (8H, m, CH₂), 6.23 (1H, br, NH), 6.33 (1H, d, H-7), 6.52 (1H, s, H-1), 7.00 (1H, d, H-6) ppm; δ_C (150 MHz, CDCl₃) 10.2 (CH₃), 18.3 (CH₃), 21.7 (CH₃), 28.6, 29.4, 30.0, 30.9, 31.1, 31.6, 33.5, 33.7, 34.9, 36.4, 38.1, 39.1, 39.3, 40.2, 43.0, 44.4, 45.0, 50.6, 69.5, 70.0, 70.1, 70.5, 70.6, 70.7, 117.0, 118.0, 119.5, 127.4, 134.0, 146.0, 164.7, 170.2, 177.7, 178.3 ppm; ESI-MS m/z 651.41 [M + H]⁺ (calcd. for C₃₇H₅₅N₄O₆⁺, m/z 651.41); UV (CH₂Cl₂) peaks at 228 and 424 nm; IR (FTIR) 3332, 2931, 2870, 2360, 2106, 1643, 1589, 1442, 1288 and 1103 cm⁻¹.

3.2. Computational Studies

The 3D X-ray crystal structure of SR Ca²⁺-ATPase complexed with thapsigargin (TG1) was retrieved from the RCSB Protein Data Bank (www.rcsb.org; accessed on 24 January 2024; PDB ID 1IWO, resolution 3.10 Å) and used in agreement with previous studies [19].

Prior to conducting site-specific docking studies, SERCA was prepared, and selected chains were isolated and considered. Further, the obtained structure was processed through the DockPrep tool of Chimera in order to eventually fix missing residues in the receptor. Ligands were built and optimized using Avogadro [33].

The site-specific molecular docking study was performed using AutoDock Vina [34,35]. The search grid was set according to the following parameters: $x = -4.5190$, $y = -25.0079$, $z = 9.5195$; size: 30.000 × 30.000 × 30.000 Å. Docking simulation was carried out with default Vina parameters; the number of generated docking poses was set to 8, and the docking energy conformation value was expressed in -kcal/mol. After the identification of the best poses, the root-mean-square deviation (RMSD) value was used to validate the adopted method with the rmsd.py script, and a score under 2.50 Å was deemed sufficient to consider the analysis accurate. In the case of this study, an RMSD value of 1.1056 Å was obtained. Schrödinger Release 2023-1: Maestro, Schrödinger, LLC, New York, NY, 2023 was used to produce the artworks.

4. Conclusions

This study introduced the synthesis of a celastrol derivative that could be utilized for profiling studies or, alternatively, for applications in click chemistry. The synthesized compound underwent characterization through NMR, UV, IR, and mass spectrometry. Computational studies were also employed to assess its binding mode within the receptor. Molecular docking results reported a similarity in the binding mode of thapsigargin and compound 4; this was also followed by the similar docking scores. Although ADME profiling reported one violation of the Lipinski's rule, the characterization of compound 4 paves the way for a promising starting point for further optimization steps.

Supplementary Materials: The following supporting information is available online. Figure S1: ¹H-NMR spectrum (CDCl₃, 600 MHz) of compound 3; Figure S2: ¹³C-NMR spectrum (CDCl₃, 150 MHz) of compound 3; Figure S3: DEPT-135 spectrum (CDCl₃, 150 MHz) of compound 3; Figure S4: ¹H-NMR spectrum (CDCl₃, 600 MHz) of compound 4; Figure S5: ¹³C-NMR spectrum (CDCl₃, 600 MHz) of compound 4; Figure S6a: HSQC spectrum (CDCl₃, 600 MHz) of compound 4; Figure S6b: An expanded view of HSQC spectrum (CDCl₃, 600 MHz) of compound 4; Figure S7: ¹H-COSY spectrum (CDCl₃, 600 MHz) of compound 4; Figure S8: DEPT-135 spectrum (CDCl₃, 150 MHz) of compound 4; Figure S9: DEPT-90 spectrum (CDCl₃, 150 MHz) of compound 4; Figure S10: DEPT-45 spectrum (CDCl₃, 150 MHz) of compound 4; Figure S11: IR spectrum (KBr) of compound 1; Figure S12: IR spectrum (FTIR) of compound 4; Figure S13: UV spectrum of compound 4 (range 200–500 nm in CH₂Cl₂); Figure S14: UPLC-UV chromatogram (254 nm) and mass spectrum of compound 4; Figure S15: Interaction of celastrol with SERCA; Table S1: ¹H and ¹³C-NMR chemical shifts and 2D structure of 4; Table S2: Physicochemical properties of compound 1 and 4 calculated by SwissADME [32].

Author Contributions: G.Y., X.Y. and R.Z. synthesized products 3 and 4 described on page 4. M.A. and G.R. are experts in computational chemistry, and they were involved in performing the

experiments detailed on page 5. Conceptualization, P.C.; methodology, G.Y., X.Y., and R.Z.; software, G.Y., M.A. and G.R.; validation, P.C.; formal analysis, X.Y.; investigation, R.Z.; data curation, G.Y.; writing—original draft preparation, G.Y., M.A., X.Y., and R.Z.; writing—review and editing, A.G., G.R., and P.C.; supervision, P.C.; project administration, P.C.; funding acquisition, P.C. All authors have read and agreed to the published version of the manuscript.

Funding: This research was funded by FDCT grants from Macao Science and Technology University to PC (Project Code: 0005-2023-RIA1) and by University of Brescia.

Data Availability Statement: Not applicable.

Acknowledgments: We thank Lao ChiChou for the mass spectrometry studies.

Conflicts of Interest: The authors declare no conflicts of interest.

References

- Kannaiyan, R.; Shanmugam, M.K.; Sethi, G. Molecular targets of celastrol derived from Thunder of God Vine: Potential role in the treatment of inflammatory disorders and cancer. *Cancer Lett.* **2011**, *303*, 9–20. [[CrossRef](#)] [[PubMed](#)]
- Allison, A.C.; Cacabelos, R.; Lombardi, V.R.M.; Álvarez, X.A.; Vigo, C. Central Nervous System Effects of Celastrol, a Potent Antioxidant and Antiinflammatory Agent. *CNS Drug Rev.* **2000**, *6*, 45–62. [[CrossRef](#)]
- Der Sarkissian, S.; Cailhier, J.; Borie, M.; Mansour, S.; Hamet, P.; Stevens, L.; Noiseux, N. Celastrol as a Novel Cardioprotective Drug. *Can. J. Cardiol.* **2013**, *29*, S331. [[CrossRef](#)]
- Yang, G.; Wang, K.; Song, H.; Zhu, R.; Ding, S.; Yang, H.; Sun, J.; Wen, X.; Sun, L. Celastrol ameliorates osteoarthritis via regulating TLR2/NF- κ B signaling pathway. *Front. Pharm.* **2022**, *13*, 963506. [[CrossRef](#)] [[PubMed](#)]
- Jang, S.Y.; Jang, S.-W.; Ko, J. Celastrol inhibits the growth of estrogen positive human breast cancer cells through modulation of estrogen receptor α . *Cancer Lett.* **2011**, *300*, 57–65. [[CrossRef](#)] [[PubMed](#)]
- Sun, H.; Xu, L.; Yu, P.; Jiang, J.; Zhang, G.; Wang, Y. Synthesis and preliminary evaluation of neuroprotection of celastrol analogues in PC12 cells. *Bioorganic Med. Chem. Lett.* **2010**, *20*, 3844–3847. [[CrossRef](#)] [[PubMed](#)]
- Liu, J.; Lee, J.; Salazar Hernandez, M.A.; Mazitschek, R.; Ozcan, U. Treatment of Obesity with Celastrol. *Cell* **2015**, *161*, 999–1011. [[CrossRef](#)] [[PubMed](#)]
- Jin, H.Z.; Hwang, B.Y.; Kim, H.S.; Lee, J.H.; Kim, Y.H.; Lee, J.J. Antiinflammatory Constituents of *Celastrus orbiculatus* Inhibit the NF- κ B Activation and NO Production. *J. Nat. Prod.* **2002**, *65*, 89–91. [[CrossRef](#)] [[PubMed](#)]
- Zhang, T.; Li, Y.; Yu, Y.; Zou, P.; Jiang, Y.; Sun, D. Characterization of Celastrol to Inhibit Hsp90 and Cdc37 Interaction. *J. Biol. Chem.* **2009**, *284*, 35381–35389. [[CrossRef](#)]
- Wong, V.K.W.; Qiu, C.; Xu, S.-W.; Law, B.Y.K.; Zeng, W.; Wang, H.; Michelangeli, F.; Dias, I.R.D.S.R.; Qu, Y.Q.; Chan, T.W.; et al. Ca²⁺ signalling plays a role in celastrol-mediated suppression of synovial fibroblasts of rheumatoid arthritis patients and experimental arthritis in rats. *Br. J. Pharmacol.* **2019**, *176*, 2922–2944. [[CrossRef](#)]
- Di Matteo, A.; Bathon, J.M.; Emery, P. Rheumatoid arthritis. *Lancet* **2023**, *402*, 2019–2033. [[CrossRef](#)] [[PubMed](#)]
- Gravallese, E.M.; Firestein, G.S. Rheumatoid Arthritis—Common Origins, Divergent Mechanisms. *N. Engl. J. Med.* **2023**, *388*, 529–542. [[CrossRef](#)] [[PubMed](#)]
- Liang, H.Y.; Yin, H.X.; Li, S.F.; Chen, Y.; Zhao, Y.J.; Hu, W.; Zhou, R.P. Calcium-Permeable Channels Cooperation for Rheumatoid Arthritis: Therapeutic Opportunities. *Biomolecules* **2022**, *12*, 1383. [[CrossRef](#)] [[PubMed](#)]
- Wong, V.K.; Li, T.; Law, B.Y.; Ma, E.D.; Yip, N.C.; Michelangeli, F.; Law, C.K.; Zhang, M.M.; Lam, K.Y.; Chan, P.L.; et al. Saikosaponin-d, a novel SERCA inhibitor, induces autophagic cell death in apoptosis-defective cells. *Cell Death Dis.* **2013**, *4*, e720. [[CrossRef](#)] [[PubMed](#)]
- Xu, S.-W.; Law, B.Y.K.; Qu, S.L.Q.; Hamdoun, S.; Chen, J.; Zhang, W.; Guo, J.-R.; Wu, A.-G.; Mok, S.W.F.; Zhang, D.W.; et al. SERCA and P-glycoprotein inhibition and ATP depletion are necessary for celastrol-induced autophagic cell death and collateral sensitivity in multidrug-resistant tumor cells. *Pharmacol. Res.* **2020**, *153*, 104660. [[CrossRef](#)]
- Lv, Q.W.; Zhang, W.; Shi, Q.; Zheng, W.J.; Li, X.; Chen, H.; Wu, Q.J.; Jiang, W.L.; Li, H.B.; Gong, L.; et al. Comparison of Tripterygium wilfordii Hook F with methotrexate in the treatment of active rheumatoid arthritis (TRIFRA): A randomised, controlled clinical trial. *Ann. Rheum. Dis.* **2015**, *74*, 1078–1086. [[CrossRef](#)] [[PubMed](#)]
- Klaić, L.; Morimoto, R.I.; Silverman, R.B. Celastrol Analogues as Inducers of the Heat Shock Response. Design and Synthesis of Affinity Probes for the Identification of Protein Targets. *ACS Chem. Biol.* **2012**, *7*, 928–937. [[CrossRef](#)] [[PubMed](#)]
- Coghi, P.; Ng, J.P.L.; Kadioglu, O.; Law, B.Y.K.; Qiu, A.C.; Saeed, M.E.M.; Chen, X.; Ip, C.K.; Efferth, T.; Liu, L.; et al. Synthesis, computational docking and biological evaluation of celastrol derivatives as dual inhibitors of SERCA and P-glycoprotein in cancer therapy. *Eur. J. Med. Chem.* **2021**, *224*, 113676. [[CrossRef](#)]
- Xie, Y.; Kuan, H.; Wei, Q.; Gianoncelli, A.; Ribaud, G.; Coghi, P. (2R,4aS,6aS,12bR,14aS,14bR)10-Hydroxy-N-(4-((6-methoxyquinolin-8-yl)amino)pentyl)-2,4a,6a,9,12b,14a-hexamethyl-11-oxo-1,2,3,4,4a,5,6,6a,11,12b,13,14,14a,14b-tetradecahydronicene-2-carboxamide. *Molbank* **2023**, *2023*, M1716. [[CrossRef](#)]
- Nasra, S.; Bhatia, D.; Kumar, A. Recent advances in nanoparticle-based drug delivery systems for rheumatoid arthritis treatment. *Nanoscale Adv.* **2022**, *4*, 3479–3494. [[CrossRef](#)]

21. Crescenzi, V.; Cornelio, L.; Di Meo, C.; Nardecchia, S.; Lamanna, R. Novel hydrogels via click chemistry: Synthesis and potential biomedical applications. *Biomacromolecules* **2007**, *8*, 1844–1850. [[CrossRef](#)]
22. Saxon, E.; Armstrong, J.I.; Bertozzi, C.R. A “traceless” Staudinger ligation for the chemoselective synthesis of amide bonds. *Org. Lett.* **2000**, *2*, 2141–2143. [[CrossRef](#)] [[PubMed](#)]
23. Saxon, E.; Bertozzi, C.R. Cell surface engineering by a modified Staudinger reaction. *Science* **2000**, *287*, 2007–2010. [[CrossRef](#)] [[PubMed](#)]
24. Kolb, H.C.; Sharpless, K.B. The growing impact of click chemistry on drug discovery. *Drug Discov. Today* **2003**, *8*, 1128–1137. [[CrossRef](#)] [[PubMed](#)]
25. Luo, P.; Liu, D.; Zhang, Q.; Yang, F.; Wong, Y.K.; Xia, F.; Zhang, J.; Chen, J.; Tian, Y.; Yang, C.; et al. Celastrol induces ferroptosis in activated HSCs to ameliorate hepatic fibrosis via targeting peroxiredoxins and HO-1. *Acta Pharm. Sin. B* **2022**, *12*, 2300–2314. [[CrossRef](#)] [[PubMed](#)]
26. Feng, Y.; Wang, W.; Zhang, Y.; Fu, X.; Ping, K.; Zhao, J.; Lei, Y.; Mou, Y.; Wang, S. Synthesis and biological evaluation of celastrol derivatives as potential anti-glioma agents by activating RIP1/RIP3/MLKL pathway to induce necroptosis. *Eur. J. Med. Chem.* **2022**, *229*, 114070. [[CrossRef](#)] [[PubMed](#)]
27. Li, N.; Chen, C.; Zhu, H.; Shi, Z.; Sun, J.; Chen, L. Discovery of novel celastrol-triazole derivatives with Hsp90-Cdc37 disruption to induce tumor cell apoptosis. *Bioorg. Chem.* **2021**, *111*, 104867. [[CrossRef](#)] [[PubMed](#)]
28. He, Q.-W.; Feng, J.-H.; Hu, X.-L.; Long, H.; Huang, X.-F.; Jiang, Z.-Z.; Zhang, X.-Q.; Ye, W.-C.; Wang, H. Synthesis and Biological Evaluation of Celastrol Derivatives as Potential Immunosuppressive Agents. *J. Nat. Prod.* **2020**, *83*, 2578–2586. [[CrossRef](#)] [[PubMed](#)]
29. Axer, A.; Hermann, S.; Kehr, G.; Clases, D.; Karst, U.; Fischer-Riepe, L.; Roth, J.; Fobker, M.; Schäfers, M.; Gilmour, R.; et al. Harnessing the Maltodextrin Transport Mechanism for Targeted Bacterial Imaging: Structural Requirements for Improved in vivo Stability in Tracer Design. *ChemMedChem* **2018**, *13*, 241–250. [[CrossRef](#)]
30. Pang, C.; Luo, J.; Liu, C.; Wu, X.; Wang, D. Synthesis and Biological Evaluation of a Series of Novel Celastrol Derivatives with Amino Acid Chain. *Chem. Biodivers.* **2018**, *15*, e1800059. [[CrossRef](#)]
31. Toyoshima, C.; Nomura, H. Structural changes in the calcium pump accompanying the dissociation of calcium. *Nature* **2002**, *418*, 605–611. [[CrossRef](#)] [[PubMed](#)]
32. Daina, A.; Michielin, O.; Zoete, V. SwissADME: A free web tool to evaluate pharmacokinetics, drug-likeness and medicinal chemistry friendliness of small molecules. *Sci. Rep.* **2017**, *7*, 42717. [[CrossRef](#)] [[PubMed](#)]
33. Hanwell, M.D.; Curtis, D.E.; Lonie, D.C.; Vandermeersch, T.; Zurek, E.; Hutchison, G.R. Avogadro: An advanced semantic chemical editor, visualization, and analysis platform. *J. Cheminform.* **2012**, *4*, 17. [[CrossRef](#)] [[PubMed](#)]
34. Eberhardt, J.; Santos-Martins, D.; Tillack, A.F.; Forli, S. AutoDock Vina 1.2.0: New Docking Methods, Expanded Force Field, and Python Bindings. *J. Chem. Inf. Model.* **2021**, *61*, 3891–3898. [[CrossRef](#)]
35. Trott, O.; Olson, A.J. AutoDock Vina: Improving the speed and accuracy of docking with a new scoring function, efficient optimization, and multithreading. *J. Comput. Chem.* **2010**, *31*, 455–461. [[CrossRef](#)]

Disclaimer/Publisher’s Note: The statements, opinions and data contained in all publications are solely those of the individual author(s) and contributor(s) and not of MDPI and/or the editor(s). MDPI and/or the editor(s) disclaim responsibility for any injury to people or property resulting from any ideas, methods, instructions or products referred to in the content.